Monitoring Structural Change in the Brain: Application to Neurodegeneration

Marc Tittgemeyer*, Gert Wollny, and Frithjof Kruggel

Abstract—**Magnetic resonance imaging (MRI) is used in clinical routine to map the brain's morphology. Structural changes due to brain growth, aging, surgical intervention or pathological processes may be detected by image registration of time-series imaging data. To monitor structural change a three step approach is pursued here: (1) rigid registration and intensity matching of an initial (reference) and follow-up MRI scans, (2) a non-rigid registration of the scans, and (3) the segmentation of the resulting displacement field. Cros-correlation is used as a similarity measure for rigid registration. Non-rigid registration is based on a fluid dynamical model. The resulting displacement fields are usually large and, therefore, hard to interpret. For a simplified but sufficient description of such vector fields, contraction mapping is proposed to detect vector field singularities. This enables the detection and analysis of singularities of any order as critical points which reflect the topology of the vector field. An application demonstrates how this method helps to increase the understanding of pathological processes in the brain.**

Keywords— **non-rigid registration, critical points, neurodegeneration, Alzheimer dementia**

I. INTRODUCTION

IMAGE registration is an important component in many neuroimaging applications. One of its basic objectives is to allow the characterisation of the morphology of different subject's brains. Another is to monitor intra-subject variations. In our application, changes of brain structure due to brain growth, aging, surgical intervention, or pathological processes are monitored by time-series examinations using magnetic resonance imaging (MRI). MR images are given as 3D matrices of intensity values. Beyond usual comparison of the image data, which is still the gold standard in clinical neuroscience, structural changes with time may be detected by non-linear registration of the imaged brain. The result of the registration algorithm is a vector field which maps one image onto another. This displacement field reflects the structural

The authors are with the Max-Planck-Institute of Cognitive Neuroscience, Stephanstr. 1a, D-04103 Leipzig, Germany (email: {tittge,wollny,kruggel}cns.mpg.de)
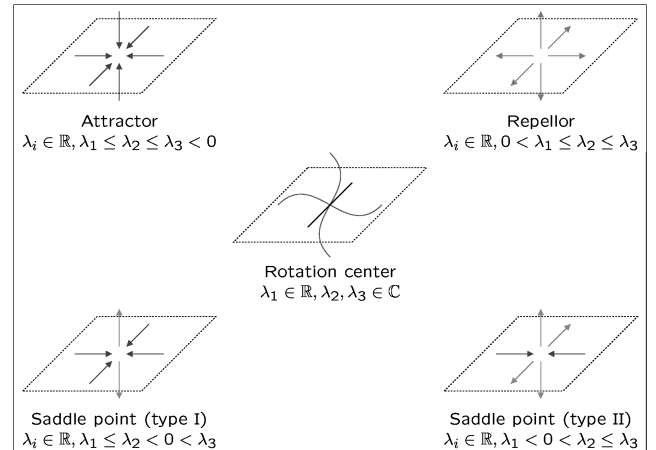
Fig. 1. Classification criteria for critical points (after [1]). λ_i denote the eigenvalues of the phase portrait to a critical point.

change that acted on the brain. Unfortunately, such vector fields are usually high-dimensional, large, and, therefore, hard to interpret.

High-dimensional vector fields are a result of observed measurements or simulated processes in a variety of application domains (e.g., geophysics, meteorology, or medicine). The characterisation of vector fields from registration of medical image sequences was stimulated by Thirion and Calmon [26]. Consecutive methods basically focus to segment areas of changing brain volume through the Jacobian [9, 24], or to detect growth pattern by tensor maps [27]. In order to improve the understanding of underlying dynamics in our measurement, we propose to characterise the vector fields by their critical points.

The most prominent critical points are attractors, repellors and vortices (rotation centers). Abraham and Shaw [1] introduced a concise classification scheme for critical points (Fig. 1) based on their phase portrait. In general, critical points characterise a high-dimensional vector field as a sparse set of features that are sufficient to understand the behaviour of the simulated physical process and its topology.

The detection and visualisation of critical points within vector fields is still an active research area

in which rather sophisticated mathematical methods have been employed [13]. Topological methods, as introduced by Helman and Hesselink [14] are established. These methods decompose a vector fields in different global regions of interest, but are usually based on local linear approximations of the Jacobian. Higher-order approximations yield different decompositions [25]. Philippou and Strickland [21] introduced a geometrical method that describes critical points at the intersection of lines tangent with the vector orientation (or at the intersection of planes orthogonal to the vectors). Other widely employed methods are based on the Poincaré-Hopf index theorem (e.g., [11]).

Due to the finite spatial resolution of the images, the displacement field is given on a discrete grid. Since, for example, growth or atrophying processes take place in finite sub-compartments of the brain, representing critical points by point sources is an over-simplification. Most conventional methods fail, therefore, to detect critical points within medical vector fields. Thus, in our application, critical points are not regarded as infinitesimally small.

We here propose a novel method that is based on the contraction mapping theorem [17]. For an application to a patient suffering from neuro-degeneration (Alzheimer's disease) we will illustrate how nonrigid registration and critical points analysis may help to understand the disease process.

II. IMAGE REGISTRATION

Image registration is usually achieved by applying a vector field transformation to one image in order to match another (reference) image with respect to a given cost function describing the image differences [18]. In practice, these transformations must accommodate both very complex and large deformations. The mathematical framework to carry out such a task with respect to the discipline of computational anatomy has been compiled by Grenander and Miller [12].

To correct for positioning and global size differences between reference and follow-up images, we first apply a rigid registration algorithm. Then, we correct for intensity scaling artifacts in the time-series examinations. Implementations for both steps were obtained from the SimBio bio-numerical simulation environment [16].

The high dimensional transformations involved in non-rigid registration generally make the problem of matching images ill-conditioned (i.e., many possible solutions exist), so that additional constraints are needed to obtain a physically plausible result [2, 3, 10, 19]. Recently, Musse et al. [20] as well as Christensen and Johnson [7] also address the topological issues involved with small and large-distance non-linear transformations.

Bio-mechanically plausible transformations are constrained to be consistent with the physical properties of deformable elastic solids. To understand how elastic image matching works, consider the deforming image to be embedded in a 3D elastic medium. The medium is subjected to distributed internal forces which reconfigure it and lead the image to match a target. In linear elastic media, the displacement vector field $\vec{u}(\vec{x})$ resulting from internal driving forces $\vec{F}(\vec{x})$ (called *body forces*) obeys the Navier-Stokes equilibrium equations for linear elasticity:

$$\mu \nabla^2 \vec{u} + (\lambda + \mu)\vec{\nabla}(\vec{\nabla} \cdot \vec{u}) = \vec{F}(\vec{u}), \quad \forall \vec{x} \in \mathbb{R}^n. \quad (1)$$

Here $\mathbb{R}^n$ is the discrete lattice representation of the image; $\vec{\nabla} \cdot \vec{u} = \partial u_j \sum /\partial x_j$ is the cubical dilatation of the medium; ∇^2 is the Lagrangian operator, and Lamé's coefficients λ and μ refer to the elastic properties of the medium: λ controls the rate of growth or shrinkage of a local region, whereas μ controls the shearing between adjacent regions of the image.

However, the assumption of linear elasticity confines the registration to be globally smooth and therefore to accommodate only small deformations. In an extension to his initial work [5], Christensen [6] described a registration approach in which a viscous fluid model was used to control the deformation.

For viscous fluids, the force $\vec{F}(\vec{u})$ is proportional to the time rate of change in displacement. The PDE describing the fluid transformation of the template is given by (refer to Christensen et al. [8] for a detailed derivation):

$$\nabla^2 \vec{v} + (\lambda + \mu)\vec{\nabla}(\vec{\nabla} \cdot \vec{v}) = \vec{F}(\vec{u}). \quad (2)$$

Here, $\vec{v}$ is the instantaneous velocity of the displacement field $\vec{u}$. It is related to its displacement $\vec{u}$ by

$$\vec{v}(\vec{x},t) = \frac{\partial \vec{u}(\vec{x},t)}{\partial t} + \vec{v}(\vec{x},t)^T \vec{\nabla} \vec{u}(\vec{x},t). \quad (3)$$

The $\nabla^2 \vec{v}$ term in (2) is the viscous term of the PDE. This term constrains the velocity of the neighbouring particles of the displacement field to vary smoothly.

Due to attenuation in viscous fluids, internal forces in this model disappear with time. Thus, the desired deformation can be fully achieved even if large deformations are required. Unfortunately, the original implementation is demanding with respect to its computational cost. Wollny and Kruggel [28] therefore proposed a fast algorithm to carry out non-rigid registration based on fluid dynamical modelling.

III. THE CONCEPT OF CRITICAL POINTS

Considering a vector field $\vec{u} : \Omega \rightarrow \mathbb{R}^3$ for any compact domain $\Omega \subseteq \mathbb{R}^3$ and the set

$$U_\varepsilon(\vec{x}') := \{\vec{x} | \parallel \vec{x} - \vec{x}' \parallel < \varepsilon, \vec{x} \in \Omega\}, \qquad (4)$$

for any $\varepsilon > 0, \varepsilon \in \mathbb{R}$ and a $\vec{x}' \in \Omega$, then U_ε is called the ε-*environment* of $\vec{x}'$.

The Taylor series expansion of $\vec{u}(\vec{x})$ around the point $\vec{x}'$ yields:

$$\vec{u}(\vec{x}) = \frac{\partial u_i}{\partial x_j}\bigg|_{\vec{x}'} (\vec{x} - \vec{x}') + \vec{u}(\vec{x}') + O(\vec{x}).$$

By taking into account only its linear terms, and with the substitution $\vec{A} := \frac{\partial u_i}{\partial x_j}\big|_{\vec{x}'}, \vec{A} \in \mathbb{R}^{3 \times 3}$, we obtain

$$\vec{u}(\vec{x}) = \vec{A}(\vec{x} - \vec{x}') + \vec{u}(\vec{x}'). \qquad (5)$$

Thus, we can now define [cf. 21]:

Definition 1: A critical point $\vec{x}_{cp}$ is an equilibrium point in the vector field topology where $\vec{u}(\vec{x}_{cp}) = 0$, while there exists an $\varepsilon > 0, \varepsilon \in \mathbb{R}$, so that $\vec{u}(\vec{x}) \neq 0 \,\forall\, \vec{x} \in U_\epsilon(\vec{x}_{cp}) \backslash \{\vec{x}_{cp}\}$.

Proposition 1: Within the vicinity of a critical point $\vec{x}_{cp}$, the vector field $\vec{u}(\vec{x})$, as outlined in (5), can be approximated by

$$\vec{u}(\vec{x}) = \vec{A}(\vec{x} - \vec{x}_{cp}),$$

where the matrix $\vec{A}$ is called the *phase portrait* of the critical point $\vec{x}_{cp}$.

Since a first-order Taylor series would have a limited scope in modelling $\vec{u}(\vec{x})$ adequately (i.e., the influence of critical point $\vec{x}_{cp}$ would decay with distance $\Delta \vec{x} = \vec{x} - \vec{x}_{cp}$) accuracy in modelling can be increased by introducing the attenuation factor $1/\parallel \vec{x} - \vec{x}_{cp} \parallel^2$. Consequently, the approximation of $\vec{u}(\vec{x})$ now reads

$$\vec{u}(\vec{x}) = \frac{1}{\parallel \vec{x} - \vec{x}_{cp} \parallel^2} \vec{A}(\vec{x} - \vec{x}_{cp}). \qquad (6)$$

A critical point may be classified with respect to the eigenvalues of $\vec{A}$ (as proposed by Abraham and Shaw [1]): we distinguish attractors, repellors, saddle points, and rotation centers (see Fig. 1).

For our intended application, namely to interpret morphological changes of the brain, attractors and repellors may describe areas of matter loss and growth; respectively, saddle points may characterise configurations at barriers or membranes, and rotation centers may indicate local tissue shearing.

IV. ESTIMATION OF CRITICAL POINTS

When registering morphological changes, we obtain vector fields (the displacements) that are not given on a continuous domain Ω, but on its discretisation $\hat{\Omega}$ which reflects the finite resolution of the images. As discussed in the introduction, a critical point in our application domain is not infinitesimally small, but merely represents a zone to which the vector field is attracted to or repelled from, for example.

In estimating critical points we rely on the contraction mapping theorem [e.g., 17]. From its mathematical foundation, contraction mapping is confined to detect attractors or repellors, only. If a saddle point is unbalanced (i.e. the inflow of matter is not equal to the outflow), or if a rotation center has additionally an attracting or repelling component, then we are able to detect this critical points by contraction mapping.

A. Estimation algorithm

The algorithm to estimate attractors and repellors can be subdivided in three steps: (1) cumulation and (2) clustering of attracting/repelling areas followed by (3) a phase portrait estimation to carry out a classification. In the following, with respect to an attractor the transformation $T : \Omega \rightarrow \Omega$ will be applied, so that

$$\vec{T}(\vec{x}) = \vec{x} + \vec{u}(\vec{x}). \qquad (7)$$

$\vec{T}$ is achieved by non-rigid registration (Sec. II) and resides in an Euclidean reference frame. Accordingly, repellors can be attributed to

$$\vec{T}_{inv}(\vec{x}) = \vec{x} - \vec{u}(\vec{x}). \qquad (8)$$

A.1 Cumulation

To find fix points $\vec{a}$ in the displacement field $\vec{u}$, we define a counter C on the discretised domain $\hat{\Omega}$. Introducing a threshold t, and

$$\hat{\Omega}_{\text{start}} := \left\{ \vec{x} \mid \parallel \vec{u}(\vec{x}) \parallel > t, \, t > 0, \, \vec{x} \in \hat{\Omega} \right\}, \quad (9)$$

yields a set of starting points, that are linked to the attraction areas $\Theta(\vec{a}) \supset \{\vec{a}\}$ (i.e., an attraction area will contain more then just one point). Now consider the sequences $\left[T^k(\vec{x}) \right]_{k=0,1,\ldots}$. When reaching the condition $\vec{u}(T^k(\vec{x})) < t$, we increment the counter $C(T^k(\vec{x}))$. The requirement for $k > k_{\max}(= 2000)$ obviates oscillations between points of accumulations. The distribution of the counter values $C(\vec{x})$ reflects the distribution of fix points of the vector field $\vec{u}$, after an iteration over all $\vec{x} \in \hat{\Omega}_{\text{start}}$.

A.2 Clustering

With two sequences $\left[T^k(\vec{x}_1) \right]_{k=0,1,\ldots}$ and $\left[T^l(\vec{x}_2) \right]_{l=0,1,\ldots}$ we will converge to the same fix point $\vec{a}$ if the following assumption is fulfilled

$$\begin{aligned} \vec{u}(T^k(\vec{x}_1)) < t \quad \wedge \\ \vec{u}(T^l(\vec{x}_2)) < t \to \left\| T^k(\vec{x}_1) - T^l(\vec{x}_2) \right\| < \alpha \quad (10) \end{aligned}$$

for a certain value $\alpha > 0, \alpha \in \mathbb{R}$. The value of α should be chosen according to resolution of the grid $\hat{\Omega}$. A suitable choice is $0.5 \times$ voxel size. The threshold value t is set to the resolution of the grid (1 mm in our case).

Attracting points are obtained by clustering the counter C: First, find a seed point $\vec{s} \in \hat{\Omega}$ with $C(\vec{s}) > t$, and create a point size cumulation area $\Theta_{\vec{s}}$ which then accumulates by adding neighbouring grid points $\vec{x}$ as long as $C(\vec{x}) > t$. After $\Theta_{\vec{s}}$ has established its final size, its center of gravity is calculated; weighted with the counter values $C(\vec{x})$, $\vec{x} \in \Theta_{\vec{s}}$ and then used as location of a critical point:

$$\vec{x}_{\text{cp}} := \frac{\sum_{\vec{x} \in \Theta_{\vec{s}}} C(\vec{x})\vec{x}}{\sum_{\vec{x} \in \Theta_{\vec{s}}} C(\vec{x})}. \quad (11)$$

Finally, at each $\vec{x} \in \Theta_{\vec{s}}$ the counter is set $C(\vec{x}) := 0$ to ensure that the same points $\vec{x}$ are not taken into account for further clustering. The procedure is repeated until $C(\vec{x}) \leq t \, \forall \, \vec{x} \in \hat{\Omega}$.
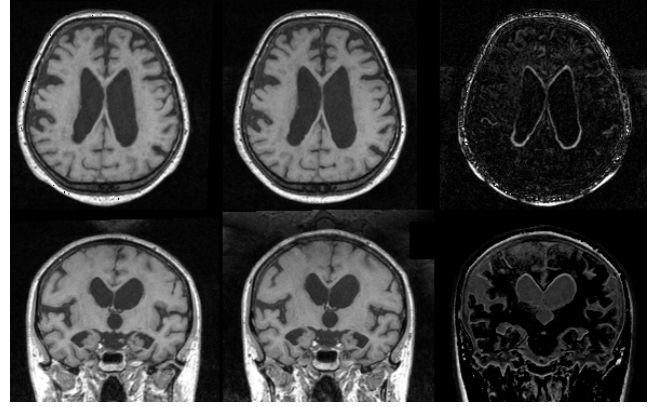

Fig. 2. Axial slice 90 (top row) and coronal slice 140 (bottom row) from $200 \times 256 \times 200$ voxel MR data sets taken 3 months (left panel) and 15 months (middle panel) after the patient's initial diagnostic findings. The right panel shows the difference between both images.

A.3 Phase Portrait Estimation and Classification

Since we are seeking for an approximation of the vector field $\vec{u}(\vec{x})$ in the environment of a critical point $\vec{x}_{\text{cp}}$, we may substitute $\Delta\vec{x} := \vec{x} - \vec{x}_{\text{cp}}$ in (6) and yield:

$$\parallel \Delta\vec{x} \parallel^2 \vec{u}(\vec{x}_{\text{cp}} + \Delta\vec{x}) = \vec{A}(\Delta\vec{x}). \quad (12)$$

Accounting for a certain environment around $\vec{x}_{\text{cp}}$, with (12) we obtain an over-determined system of linear equations [21] which can be solved by using Householder transformations [23]. Since the phase portrait A is a 3×3 matrix, its eigenvalues can be calculated easily by solving the characteristic equation

$$\det(\vec{A} - \lambda\vec{I}) = 0$$

using Cardan's formula [4]. Critical points are classified by examining their eigenvalues (see Fig. 1).

V. Application—Visualisation of Shape Change

We applied our algorithm to magnetic resonance (MR) images of a patient suffering from a neurodegenerative disease (Alzheimer's disease). Analysing the pattern of tissue loss is important for a better understanding of the pathological process induced by the disease.

A patient was scanned twice within 12 months (Fig. 2). Both datasets were registered by the fluid dynamic, non-rigid approach described in Section II. We obtained a displacement vector at each point of the reference image which corresponds to the shift
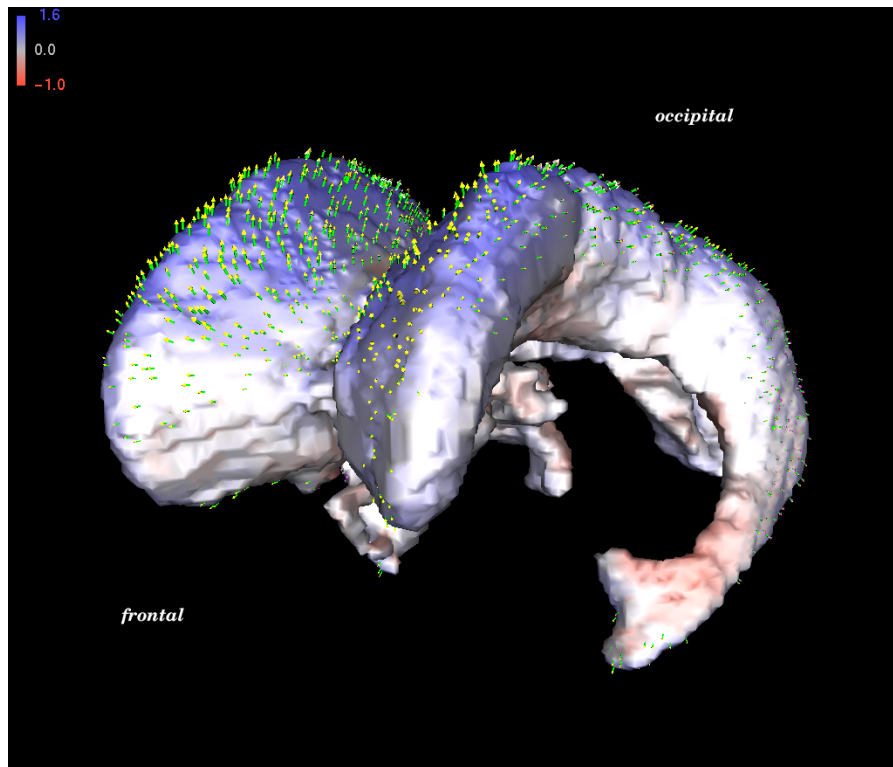
Fig. 3. Shape difference of a patient's ventricular system between two examination time points (see text). Colour indicates the orientation and magnitude of shape difference; arrows indicate the displacements. Note the overall enlargement of the system which is a consequence of tissue loss (atrophy) of the surrounding brain.
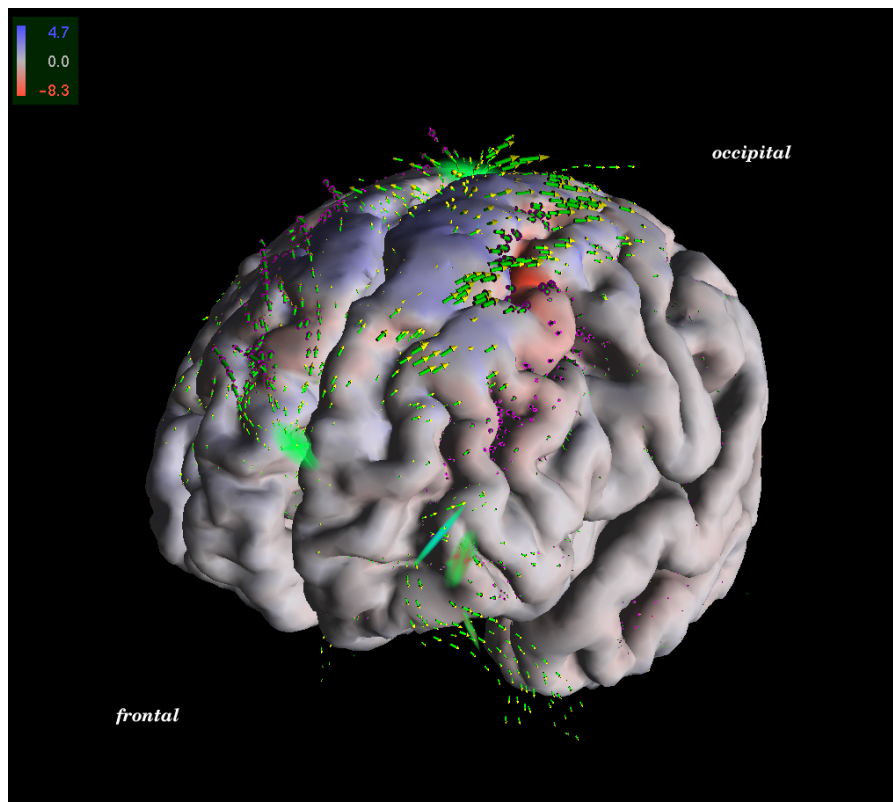

Fig. 4. Pattern of shape changes of a patient's brain between two examination time points. Morphological changes are colour coded; red and blue indicate inward and outward direction, respectively, and intensity corresponds to the magnitude of shape change perpendicular to the surface of the brain. The major displacement lines (arrows) depict the deformation lines. The critical point (repellor) within the frontal CSF compartment indicates a virtual flow in fronto-occipital direction.
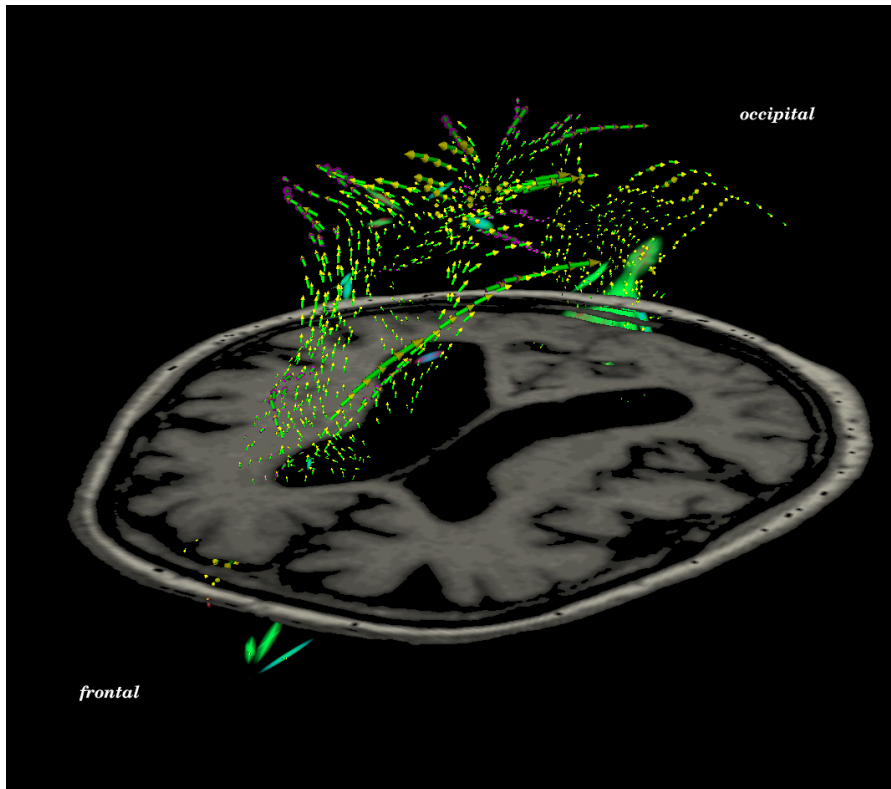
Fig. 5. View of an axial slice (taken from Fig. 4) with major displacement lines and critical points of high magnitude. A repellor (green object) in the frontal cerebrospinal fluid (CSF) and the displacement lines depict a virtual flow in occipital direction. Saddle points of type II (cf. Fig. 1) with strong repelling properties were found within the occipital CSF, and reveal a retraction of the brain. Small attractors (red) some with rotation properties (red-magenta) presumably correspond to areas of a regionally more profound matter loss.

of tissue during the time interval. Fig. 3 serves as a first example to visualise such morphological change. The ventricular system (the low-intense cavities within the brain in Fig. 2) was segmented from the brain. The spatial pattern of shape change was visualized as follows: For each point on the ventricular surface, the displacement vector is decomposed into its normal and tangential components. Inward-pointing normals are coded in red, outward-pointing in blue; colour intensity reflects its magnitude. The scale is given in mm. The displacement vectors are shown as arrows. It is interesting to note that the ventricles are clearly enlarged, most notably in a superior direction, which which indicates a more profound tissue loss in the supra-ventricular compartment.

We extracted (in total 110) critical points from the displacement field. To represent their properties, a colour scheme was implemented. Green indicates repelling (red: attracting) properties, blue a rotation component. Different types of saddle points may be distinguished by mixing the respective colours.

The set of critical points is dominated by a strong repellor located in the pre-frontal CSF compartment (Fig. 4), and by several saddle points with strong repelling properties within the occipital CSF compartment (Fig. 5). A focus of matter loss is in the frontal lobes, leading to an increase of the CSF component close to the frontal pole. Displacement stream lines (Figs. 4 and 5) map the "flow" of tissue along the midline structures (as a correlate to global atrophy) and reveal a retraction of the brain in the frontal-occipital direction. The occipital saddle point (Fig. 5) can be interpreted as a backward shift of the brain, while pushing CSF in the repelling direction. As could be deduced by Fig. 4, the strongest deformations occur in the posterior portions of the first and second frontal gyrus on both hemispheres.

VI. CONCLUSION

We proposed to monitor structural changes in the brain by non-rigid registration of time-series of MR images. To describe the resulting displacement fields we focussed on its critical points. We introduced a novel method for finding critical points in discrete

vector fields, that is based on contraction mapping.

However, our method fails to detect some specific critical points, such as rotation centers or balanced saddle points. Here, local measures based on the Jacobian [15] or global approaches such as those recently introduced by Polthier and Preuß [22] will be integrated with this method.

The advantage of conducting a biomedical analysis over simple visual comparison as carried out in clinical routine is obvious: the consequences of neurodegenerative disease are understood as a circumscribed tissue loss leading to quantifiable deformations of the brain structures.

REFERENCES

[1] R. H. Abraham and C. D. Shaw. *Dynamics–The Theory of Behavior*. Addison-Wesley, Redwood (Ca), 2nd edition, 1992.

[2] Y. Amit. A nonlinear variational problem for image matching. *Soc. Ind. Math.*, 15(1):207–224, 1994.

[3] F. L. Bookstein. Landmark methods for forms without landmarks: morphometrics of group differences in outline shape. *Med. Image Anal.*, 1(3):225–243, 1997.

[4] I. N. Bronstein, K. A. Semendjajev, G. Musiol, and H. Mühlig. *Taschenbuch der Mathematik (in german)*. Verlag Harry Deutsch, Thun · Frankfurt/M., 5th edition, 2001.

[5] G. E. Chistensen, R. D. Rabbit, and M. I. Miller. 3D brain mapping using deformable neuroanatomy. *Phys. Med. Biol.*, 39:609–618, 1994.

[6] G. E. Christensen. *Deformable shape models for neuroanatomy*. DSc.-thesis, Server Institue of Technology, Washington University, Saint Louis, 1994.

[7] G. E. Christensen and H. J. Johnson. Consistent image registration. *IEEE Trans. Med. Imag.*, 20(7):568–582, 2001.

[8] G. E. Christensen, R. D. Rabbitt, and M. I. Miller. Deformable templates using large deformation kinematics. *IEEE Trans. Med. Imag.*, 5(10):1435–1447, Oct. 1996.

[9] M. K. Chung, K. J. Worsley, T. Paus, C Cherif, D. L. Collins, J. N. Giedd, J. L. Rapoport, and A. C. Evans. A unified statistical approach to deformation- based morphometry. *NeuroImage*, 14:595–606, 2001.

[10] J. C. Gee, M. Reivich, and R. Bajcsy. Elastically deforming atlas to match anatomical brain images. *J. Comput. Ass. Tomogr.*, 17:255–236, 1993.

[11] D. H. Gottlieb and G. Samaranayake. The index of discontinuous vector fields. *New York J. Math.*, 1:130–148, 1995.

[12] U. Grenander and M. I. Miller. Computational anatomy: An emerging discipline. *Quaterly Appl. Math.*, LVI(4):617–694, Dec. 1998.

[13] H.-C. Hege and K. Polthier, editors. *Mathematical visualization : Algorithms, applications and numerics*. Springer, Berlin, 1998.

[14] J. L. Helman and L. Hesselink. Representation and display of vector field topology in fluid flow data sets. *IEEE Computer*, 22(8):27–36, August 1989.

[15] J. L. Helman and L. Hesselink. Visualizing vector field topology in fluid flows. *IEEE Comput. Graph. Appl.*, 11(3):36–46, May 1991.

[16] F. Kruggel and D. Barber. Image processing design report. Technical Report Deliverable 1.1a, http://www.ccrl-nece.de/simbio/ReportsEvents/deliverables.shtml, 2000.

[17] N. Lu. *Fractal Imaging*. Academic Press, San Diego, CA, 1997.

[18] J. B. A. Maintz and M. A. Viergever. A survey of medical image registration. *Medical Image Analysis*, 2(1):1–36, 1998.

[19] M. I. Miller, G. E. Christensen, Y. Amit, and U. Grenander. Mathematical textbook of deformable neuroanatomies. In *Proc. Natl. Acad. Sci. USA 90*, pages 11.944–11.948, 1993.

[20] O. Musse, F. Heintz, and J.-P. Armspach. Topology preserving deformable image matching using constraint hierachical parametric models. *IEEE Trans. Med. Imag.*, 10(7):1081–1093, July 2001.

[21] P. A. Philippou and R. N. Strickland. Vector Field Analysis and Synthesis Using Three-Dimensional Phase Portraits. *Graph. Mod. Imag. Process.*, 6(59):446–462, 1997.

[22] K. Polthier and E. Preuß. Detecting vector field singularities from potentials. http://www-sfb288.math.tu-berlin.de/~konrad/articles.html, 2001.

[23] W. H. Press, S. A. Teukolsky, W. T. Vetterling, and B. P. Flannery. *Numerical Recipes in C. The*

Art of Scientific Computing. Cambridge Univ. Press, New York, 2nd edition, 1992.

[24] D. Rey, G. Subsol, H. Delingette, and N. Ayache. Automatics detection and segmentation of evolving processes in 3D medical images: application to multiple sclerosis. In A. Kuba, M. Šámal, and A Todd-Pokropek, editors, *Information Processing in Medical Imaging*, volume 1613 of *Lect. Notes Comp. Sci.*, pages 154–167, Berlin · Heidelberg, 1999. Springer-Verlag.

[25] G. Scheuermann, H. Hagen, and H. Krüger. Clifford algebra in vector field visualization. In H.-C. Hege and K. Polthier, editors, *Mathematical Visualization*, pages 343–351. Springer-Verlag, Heidelberg, 1998.

[26] J. P. Thirion and G. Calmon. Deformation analysis to detect and quantify active lesions in 3D medical image sequences. Research Report 3101, INRIA, 1997.

[27] P. M. Thompson, J. N. Giedd, R. P. Woods, D. MacDonals, A. C. Evans, and A. W Toga. Growth patterns in the developing human brain detected using continuum mechanical tensor mapping. *Nature*, 404(6774):190–193, March 2000.

[28] G. Wollny and F. Kruggel. Computational cost of non-rigid registration algorithms based on fluid dynamics. IEEE Trans. Med. Imag., accepted.